The interannual precipitation variability in the southern part of Iran as linked to large-scale climate modes

Farnaz Pourasghar · Tomoki Tozuka ·
Saeed Jahanbakhsh · Behrooz Sari Sarraf ·
Hooshang Ghaemi · Toshio Yamagata

Abstract The interannual variation of precipitation in the southern part of Iran and its link with the large-scale climate modes are examined using monthly data from 183 meteorological stations during 1974–2005. The majority of precipitation occurs during the rainy season from October to May. The interannual variation in fall and early winter during the first part of the rainy season shows apparently a significant positive correlation with the Indian Ocean Dipole (IOD) and El Niño-Southern Oscillation (ENSO). However, a partial correlation analysis used to extract the respective influence of IOD and ENSO shows a significant positive correlation only with the IOD and not with ENSO. The southeasterly moisture flux anomaly over the Arabian Sea turns anti-cyclonically and transport more moisture to the southern part of Iran from the Arabian Sea, the Red Sea, and the Persian Gulf during the positive IOD. On the other hand, the moisture flux has northerly anomaly over Iran during the negative IOD, which results in reduced moisture supply from the south. During the latter part of the rainy season in late winter and spring, the interannual variation of precipitation is more strongly influenced by modes of variability over the Mediterranean Sea. The induced large-scale atmospheric circulation anomaly controls moisture supply from the Red Sea and the Persian Gulf.

Keywords Interannual variation · Precipitation · IOD · ENSO · Iran

1 Introduction

The interannual variability of precipitation is very important for biological and agricultural activities. Because of its low annual mean precipitation, Iran is commonly regarded as an arid country. However, this is a climatic simplification, because precipitation varies significantly in space and time (Domroes et al. 1998). El Niño/Southern Oscillation (ENSO) has been considered to be one of the most important causes of the interannual variation in rainfall over Iran (Nazemosadat and Cordery 2000; Nazemosadat 2001; Ghasemi 2003; Nazemosadat et al. 2006). For instance, Nazemosadat and Ghasemi (2004) reported that warm ENSO phases substantially reduce (enhance) the intensity and probability of the drought (wet) period in fall, particularly in southern districts. On the other hand, when La Niña condition prevails, the probability of severe drought increases in fall. In winter, the response of rainfall to ENSO events is generally weaker.

On the other hand, Ghasemi and Khalili (2008) found a link with the North Sea–Caspian pattern (NCP) and Western Mediterranean Oscillation (WeMO). Also, Razeí et al. (2011) reported that the spatial distribution of precipitation over Iran is largely governed by geographical position of both the mid-troposphere trough over the Middle East and

F. Pourasghar · S. Jahanbakhsh · B. Sari Sarraf
Department of Physical Geography, Faculty of Humanities
and Social Science, The University of Tabriz, Tabriz, Iran

T. Tozuka · T. Yamagata (✉)
Department of Earth and Planetary Science, Graduate School
of Science, The University of Tokyo, 7-3-1, Hongo,
Bunkyo-ku, Tokyo 113-0033, Japan
e-mail: yamagata@eps.s.u-tokyo.ac.jp

H. Ghaemi
Iran Meteorological Organization, Tehran, Iran

T. Yamagata
Application Laboratory/JAMSTEC, Yokohama,
Kanagawa, Japan

the Arabian anticyclone. However, relatively few studies have focused on the influence of the Indian Ocean climate variability even though it is a source of moisture.

The Indian Ocean dipole (IOD; Saji et al. 1999) is a large-scale climate mode that seriously influences many nations around the Indian Ocean rim, as well as global climate system (see also Webster et al. 1999). During a positive event, the sea surface temperature (SST) is anomalously cool in the east and warm in the west, and it is associated with the equatorial easterly anomaly (Yamagata et al. 2004). The role of IOD in climate variability on many parts of the globe has been discussed in a number of papers

(Ashok et al. 2001, 2003; Zubair et al. 2003; Saji and Yamagata 2003; England et al. 2006). For example, Chakraborty et al. (2006) have analyzed the influence of the IOD on Saudi Arabia, and demonstrated an increase in atmospheric moisture flux through the enhancement of the synoptic variability called the Arabian cyclone during positive IOD events. Yuan et al. (2009, 2011) showed that the Tibetan snow cover in early winter is positively correlated with the IOD. However, no study to date has investigated the influence of the IOD on the precipitation over the southern part of Iran. Therefore, the goal of the study is first to identify the role of the IOD on the seasonal

Fig. 1 **a** Topography map of Iran and geophysical study area, **b** precipitation climatology in the southern part of Iran from October 1974 to May 2005
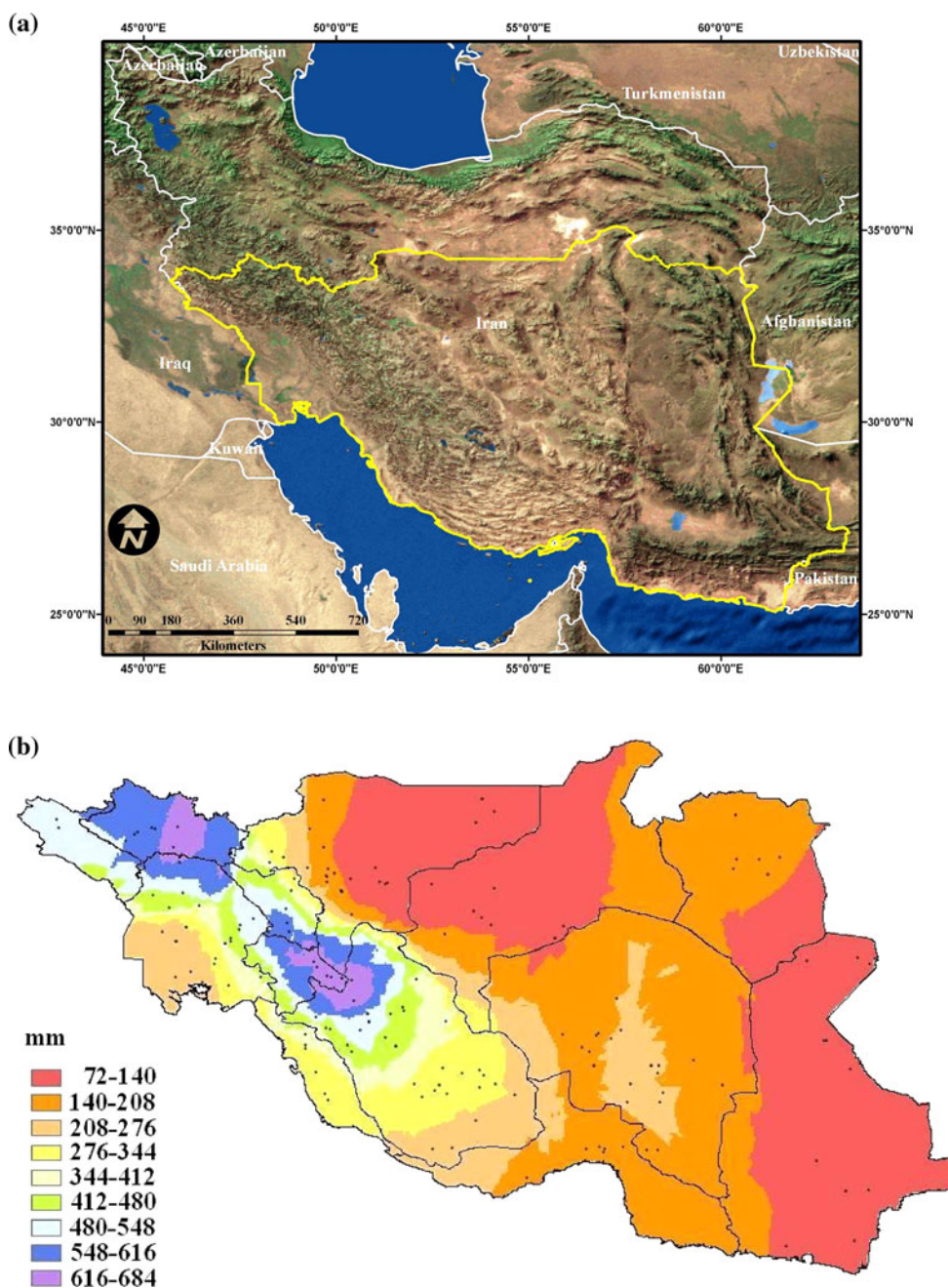
variation in precipitation over the southern part of Iran and then to examine the mechanism of interannual variation in precipitation. A brief description of data used in this study is given in the next section. In Sect. 3, we examine the seasonal variation of precipitation over the southern part of Iran to identify the rainy season. The interannual variation and its possible mechanisms are discussed in Sects. 4 and 5, respectively. The last section summarizes the main results.

2 Data

Monthly precipitation data from 183 stations in the southern part of Iran were made available by the Iranian Metrological Organization and the Iranian Water Resource Institute. The SST data used in the present study is the Hadley Centre sea ice and sea surface temperature (HADISST; Rayner et al. 2003). It is monthly data with $1° \times 1°$ horizontal resolution. The NCEP/NCAR reanalysis data (Kalnay 1996) is used for wind and specific humidity. For all data, we adopted the period from October 1974 to May 2005.

3 Precipitation climatology of the southern part of Iran

Southern Iran comprises an area of 25–35°N, 45–64°E. The Zagros Mountains in the west, the Persian Gulf and the Oman Sea to the south, and two very dry deserts in central Iran have helped to shape precipitation regimes (Fig. 1a). There are 13 provinces in the southern part of Iran. Most of the water resource of the entire country is provided by the Zagros Mountains and three large rivers, which are located in the southwestern part of Iran. Therefore, social, environmental and agricultural vulnerability highly depend on the drought severity in this region. Figure 2 shows the seasonal precipitation climatology from October 1974 to May 2005 for every province. About 98 percent of the annual precipitation occurs in October–May in 12 out of 13 provinces in the southern part of Iran. In the southeastern province, a weak precipitation maximum occurs in summer, but about 90 % of precipitation occurs between October and May. Thus, we select a rainy season from October to May. It is clear that a strong gradient exists with higher values in the western part of Iran and lower values towards the southeastern and central parts of Iran (Fig. 1b).

4 Interannual variation

To capture the dominant mode of interannual variability, we have applied the EOF analysis to detrended monthly precipitation anomaly data from 183 stations. Figures 3

and 4 show the monthly-stratified spatial patterns and principal components of the first EOF mode from October to May. We have also shown results for October–December (OND) and January-May (JFMAM). Except for May (38.8 %), more than 50 % of the total variance is explained by the first mode. Thus, the first EOF mode is a good indicator for interannual variation of precipitation. In general, stations in the mountainous region to the west around Zagros Mountains have larger loadings, suggesting that topography plays an important role in distribution of precipitation anomaly. Also, we note that the precipitation magnitude is larger in the middle of rainy season from December to March.

We then calculated correlation coefficient between the SST anomaly and the principle component of the first EOF mode for each month from October to May to obtain a clue

Table 1 Climate mode indices

Index	Definition
DMI	SSTA (40°–60°E, 10°S–10°N) − SSTA (90°–110°E, 10°S-Equator)
Niño-3	SSTA over (90°–15°W, 5°S–5°N)
IOBM	SSTA over (40°–100°E, 20°S–20°N)
WIO	SSTA over (40°–70°E, 20°S–20°N)
TAO	SSTA over (310°–342°E, 3°–22°N)
AMM	SST and wind components (10 m) (21°S–32°N, 74°W–15°E)
NAO	RPCs of NH Mean 700 hPa heights
WeMO	SLP (45°24′N–11°47′E, 36°17′N–6° 07′W)
EMI	SSTA (165°E–140°W, 10°S–10°N) − 0.5[SSTA (110°–70°W, 15°S–5°N)] − 0.5[SSTA (125°–145°E, 10°S–20°N)]

The symbols in the definition are as follows: *SST* sea surface temperature, *SSTA* sea surface temperature anomaly, *RPCs* rotated principle component, *NH* Northern hemisphere, *SLP* surface level pressure

Table 2 Correlation and partial correlation coefficients of the first EOF mode with DMI and Niño-3 index

EOF1	Correlation with		Partial correlations with	
	DMI	Niño3	DMI	Niño3
Oct	0.565[**]	0.481[**]	0.346	0.081
Nov	0.452[**]	0.297	0.371[*]	−0.101
Dec	0.103	0.099	0.041	0.031
Jan	−0.112	0.107	−0.312	0.311
Feb	−0.086	0.031	−0.175	0.156
Mar	−0.095	0.135	−0.321	0.334
Apr	−0.131	0.026	−0.242	0.206
May	−0.064	−0.051	−0.039	−0.001
OND	0.451[**]	0.339	0.316	−0.020

* (**) Significant at 95 % (99 %) by *t* test

Fig. 2 Seasonal precipitation climatology in every province in the southern part of Iran from October 1974 to May 2005

about causes of the interannual variation (Fig. 5). In October and November, positive correlations are found over the eastern tropical Pacific and the western tropical Indian Ocean, and negative correlations are found over the eastern tropical Indian Ocean and the Indonesian seas. In fact, a simple correlation coefficient calculated between the DMI (Niño-3 index) defined in Table 1 and principle components is 0.565 (0.481) for October and 0.452 (0.371) for November (Table 2). These values apparently suggest that the interannual variation of precipitation during these two months may be related with the IOD and/or ENSO.

However, we need to be careful in use of the simple correlation technique (Yamagata et al. 2004), because some IOD and ENSO events co-occur. To extract the respective influence of IOD and ENSO by assuming the independence, we here calculate a partial correlation, which is given by

$$r_{13,2} = (r_{13} - r_{12} \cdot r_{23}) \Big/ \sqrt{(1 - r_{12}^2)(1 - r_{23}^2)} \qquad (1)$$

Here, $r_{13,2}$ is the partial correlation between variable 1 and variable 3 without influence from variable 2 and r_{13}, r_{12},
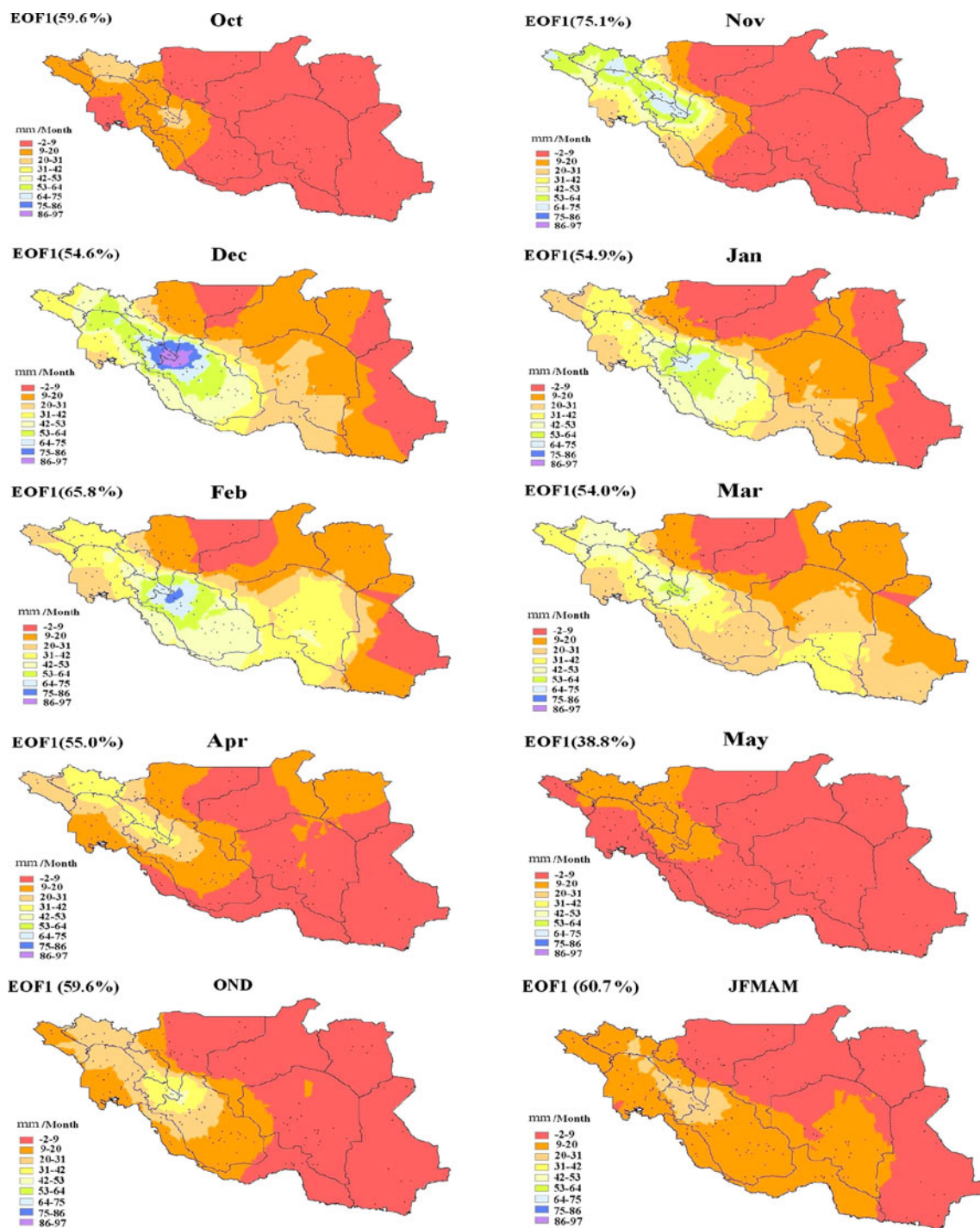
Fig. 3 Spatial pattern of EOF1 for each month from October to May, OND, and JFMAM. The variance contributions are shown in *parentheses*

and r_{23} are correlation coefficients between the variables 1 and 3, 1 and 2, and 2 and 3, respectively. The partial correlation between the first EOF mode and the DMI (Dipole Mode Index) after removing the contribution from the Niño-3 index is 0.316 for OND, whereas that between the first EOF mode and the Niño-3 index after removing the contribution from the DMI is −0.020. Thus, the interannual variation of rainfall over southern Iran during the first part

of rainy season is more closely linked with the IOD, and the positive correlation with the Niño-3 index is just a reflection of positive correlation between the DMI and the Niño-3 index. This is contrasted with the previous studies that suggested the apparent connection with ENSO.

Since the IOD decays in boreal winter and no statistically significant correlation is found in the latter part of the rainy season (Table 2), we need to seek for other climate

modes that influence the interannual variation of rainfall. For this purpose, we compute correlation between the SST anomaly and the principle component of the first EOF mode for JFMAM (Fig. 6).

We find positive correlations in addition to some positive ENSO signal in the tropical Pacific, the tropical Indian Ocean, the tropical North Atlantic, and the western Mediterranean Sea. Based on the above, we have performed correlation analysis with Indian Ocean Basin Mode Index (IOBMI; Yang et al. 2007), Western Indian Ocean Index (WIOI), Tropical Atlantic Ocean Index (TAOI), Atlantic Meridional Mode Index (AMMI; Chiang and Vimont 2004; Doi et al. 2010), North Atlantic Oscillation Index (NAOI; Barnston and Livezey 1987), El
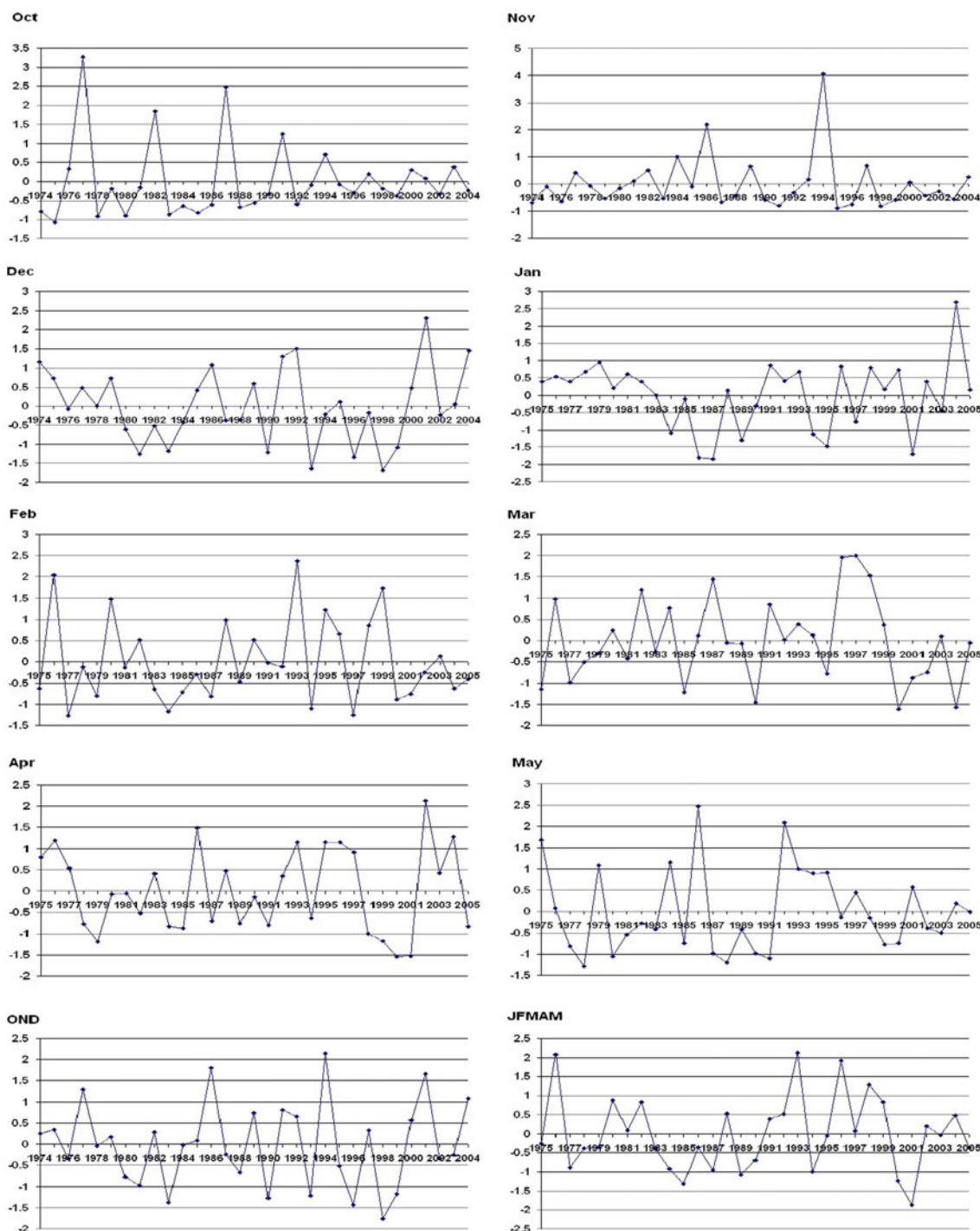

Fig. 4 Normalized principle component of EOF1 for each month from October to May, OND and JFMAM

Niño Modoki Index (EMI; Ashok et al. 2007; Weng et al. 2007) and Western Mediterranean Oscillation Index (WeMOI; Martin-Vide and Lopez-Bustins 2006) to check

possible connections with large-scale climate modes except for ENSO (Table 3).

The strongest correlation with the principle component of the first EOF mode is found for WeMOI; the correlation
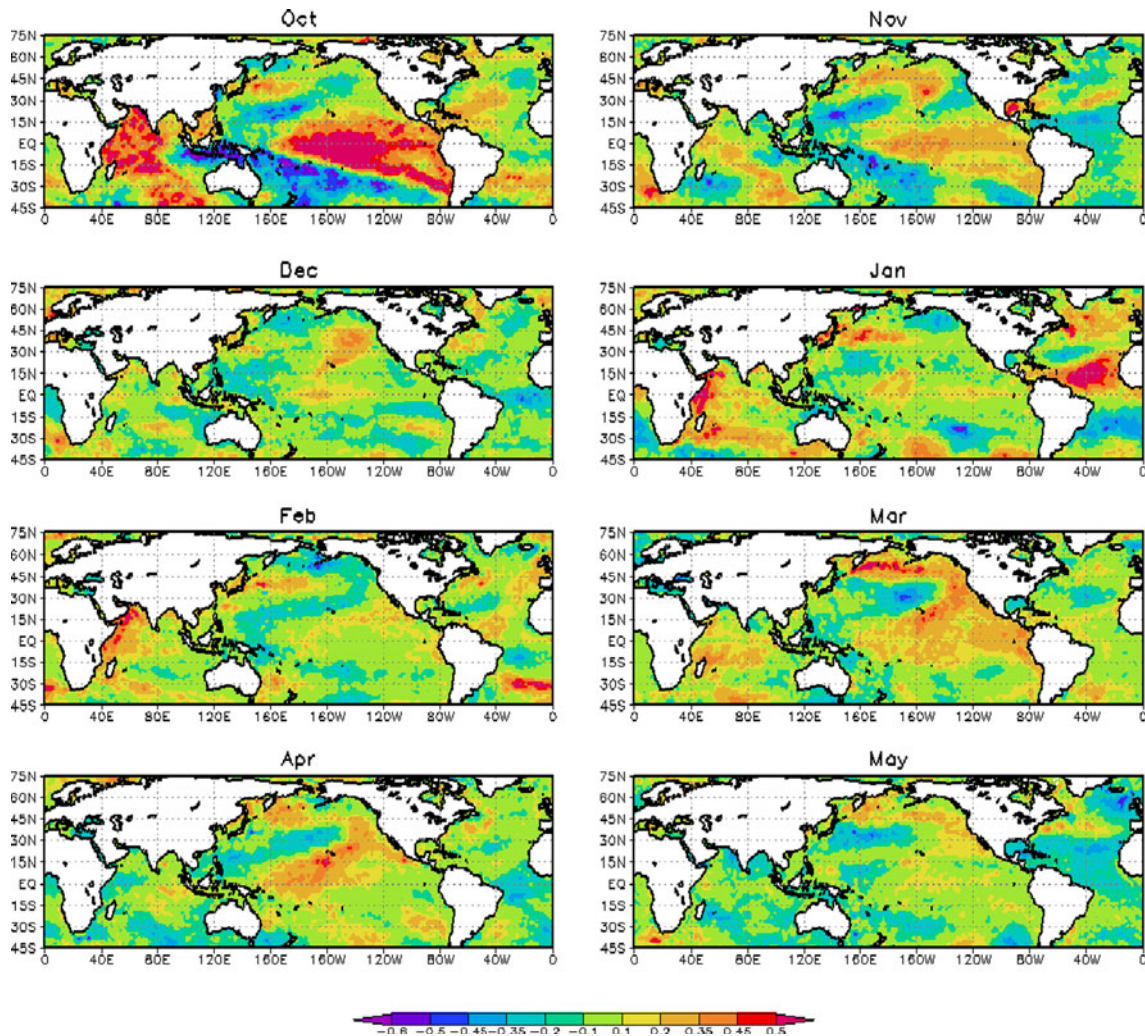

Fig. 5 Distribution of normal correlation coefficient between SST anomaly and the principle component of EOF1 for October to May. The values of ± 0.35 and ± 0.45 are at 95 and 99 % confidence level by two-tailed t test
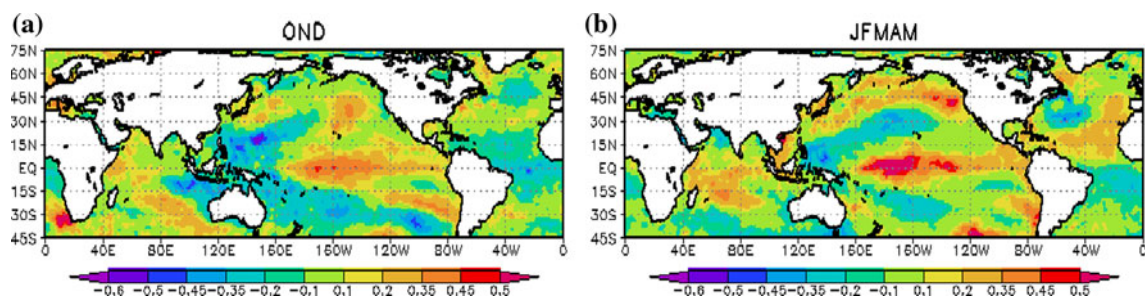

Fig. 6 Distribution of normal correlation coefficient between the SST anomaly and the principle component of EOF1 for **a** OND and **b** JFMAM. The values of ± 0.35 and ± 0.45 are at 95 and 99 % confidence levels by two-tailed t test

Table 3 Simple and partial correlation coefficients of first EOF mode with DMI, IOBMI, WIOI, TAOI, AMMI, NAOI, WeMOI, EMI

EOF1	DMI	IOBMI	WIOI	TAOI	AMMI	NAOI	WeMOI	EMI
Oct	0.565**	0.556**	0.537**	0.031	−0.126	−0.052	−0.332	0.262
Nov	0.452**	0.068	0.103	−0.381*	−0.387*	0.187	−0.243	0.164
Dec	0.103	0.006	0.028	−0.038	0.010	−0.023	−0.261	0.233
Jan	−0.112	0.264	0.459**	0.551**	0.424*	−0.147	−0.205	0.130
Feb	−0.086	0.216	0.382	0.104	0.076	0.083	−0.257	0.116
Mar	−0.095	0.193	0.103	0.066	0.031	−0.132	−0.374*	0.224
Apr	−0.131	−0.034	−0.163	−0.054	−0.044	−0.043	−0.425*	0.308
May	−0.064	−0.144	−0.065	−0.276	−0.226	0.077	−0.255	0.101
OND	0.451**	0.061	0.118	−0.257	−0.273	0.300	−0.211	0.291
JFMAM	−0.167	0.14	0.248	0.283	0.251	−0.087	−0.505**	0.298

* (**) significant at 95 % (99 %) by t test

Fig. 7 Composites of moisture flux anomaly in OND during **a** wet and **b** dry years (Unit: kg m^{-1} s^{-1}, vectors are plotted only where they are significant at the 90 % confidence level) and moisture flux anomaly divergence (Unit: 10^{-4} kg m^{-2} s^{-1}). **c** Climatology of moisture flux in OND
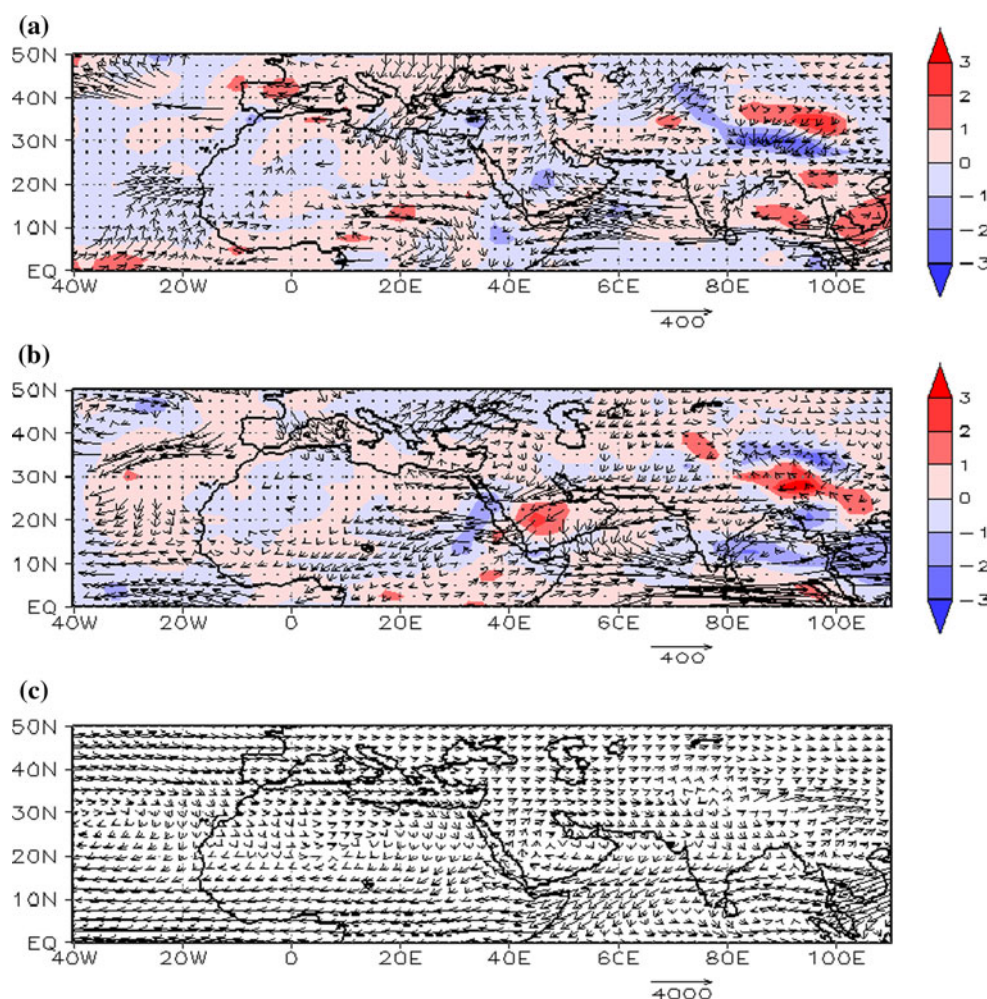

Table 4 Dry and wet years in OND -JFMAM

Months	Wet years	Dry years
OND	1977, 1986, 1991, 1994, 2001, 2004	1981, 1983, 1990, 1993, 1996, 1998, 1999
JFMAM	1976, 1980, 1982, 1993, 1996, 1998, 1999	1977, 1984, 1985, 1987, 1989, 1994, 2000, 2001

coefficient is −0.505 for JFMAM, which is significant at 99 % confidence level. Therefore, the WeMO may play an important role in modulating rainfall over the southern part of Iran during the latter part of the rainy season. Also, the correlation coefficient with the WIOI is 0.459 in January and 0.382 in February, and that with the TAOI is 0.551 and the AMMI is 0.424 in January. Thus, these climate modes may also play a role, but the correlation coefficients with these indices are not significant at 95 % confidence level for JFMAM.

5 Mechanism

To investigate the mechanism in detail, the moisture flux vector (Q_u, Q_v) defined by

$$Q_u = \frac{1}{g} \int_{P_{top}}^{P_{surf}} qu\,dp, \quad Q_v = \frac{1}{g} \int_{P_{top}}^{P_{surf}} qv\,dp, \tag{2}$$

is calculated. Here, p is pressure, P_{surf} is the surface pressure, P_{top} is the pressure of the top moisture layer (300 hPa in the NCEP/NCAR reanalysis data), q is the specific humidity, and (u, v) are zonal and meridional velocity components. Also, the contribution of anomalous advection of climatological moisture

$$Q_u' = \frac{1}{g} \int_{P_{top}}^{P_{surf}} \bar{q}u'\,dp, \quad Q_v' = \frac{1}{g} \int_{P_{top}}^{P_{surf}} \bar{q}v'\,dp, \tag{3}$$

and climatological advection of anomalous moisture

$$Q_u' = \frac{1}{g} \int_{P_{top}}^{P_{surf}} q'\bar{u}\,dp, \quad Q_v' = \frac{1}{g} \int_{P_{top}}^{P_{surf}} q'\bar{v}\,dp, \tag{4}$$

are calculated. Here, $\bar{q}(q')$, $\bar{u}(u')$ and $\bar{v}(v')$ are the climatology (anomaly) of specific humidity and zonal and meridional velocity components, respectively.
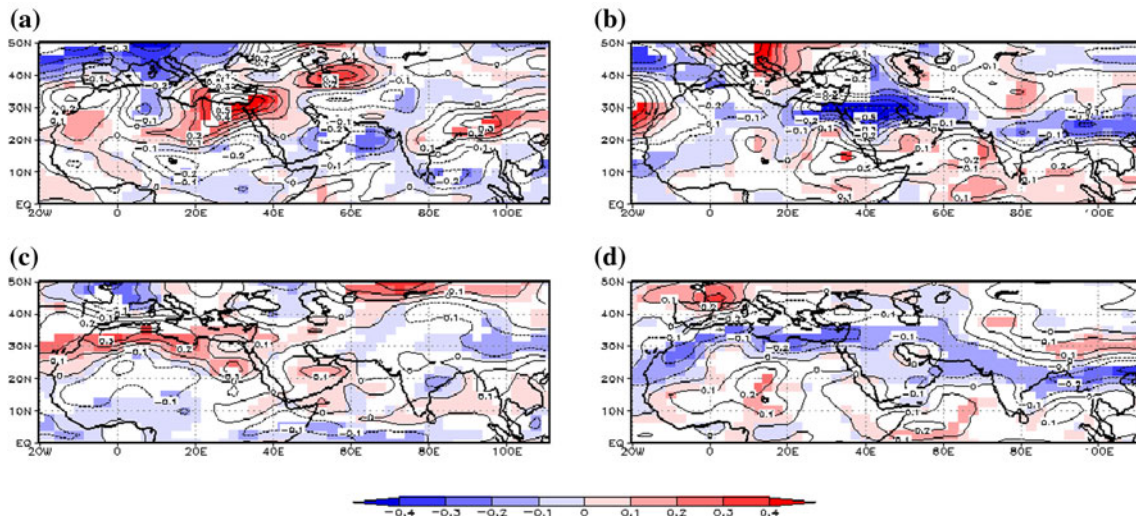

Fig. 8 Composites of the relative vorticity anomaly at 500 hPa (in 10^{-5} s^{-1}) during **a** wet and **b** dry years in OND, and **c** wet and **d** dry years in JFMAM. Anomalies exceeding 90 % confidence level are *shaded*
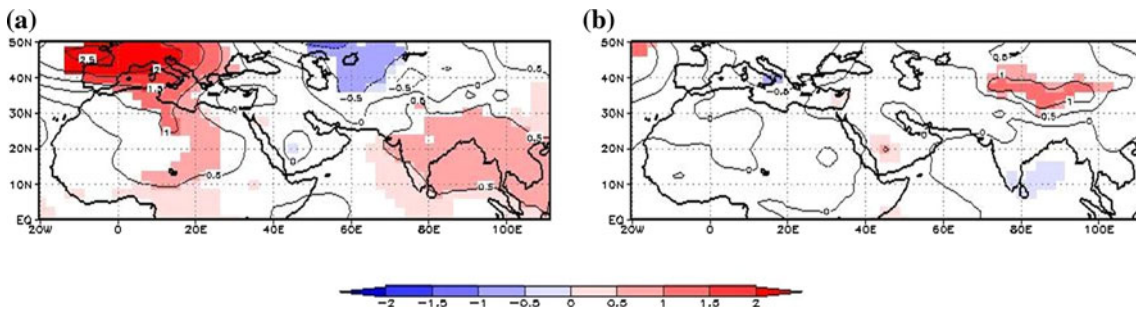

Fig. 9 Composites of SLP anomalies (in hPa) for **a** wet and **b** dry years in OND. Anomalies exceeding 90 % confidence level are *shaded*

5.1 First part of the rainy season (OND)

Prior to examining the moisture flux anomaly, it is important to understand the climatological moisture flux. The Arabian anticyclone has important role in controlling the spatial pattern of precipitation over Iran. In autumn,
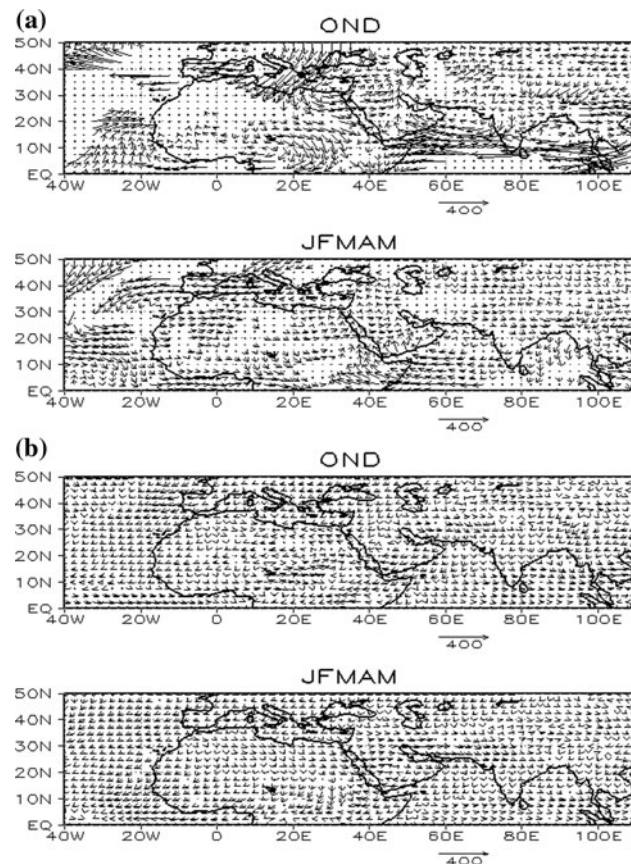

Fig. 10 Composites of moisture flux anomaly for wet years: **a** anomalous advection of moisture and **b** advection of anomalous moisture in OND and JFMAM (Unit: kg m^{-1} s^{-1}, vectors are plotted only where they are significant at the 90 % confidence level)

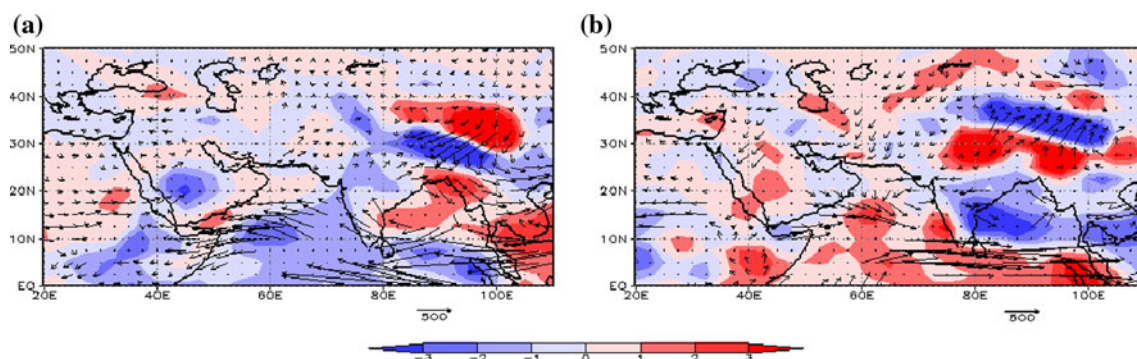when cyclone tracks are at higher latitudes and the Arabian anticyclone is still at its summer-mean position, the axis is north of the Arabian Peninsula (Razei et al. 2011).

The climatological moisture flux during the first part of the rainy season (i.e. OND) is shown in Fig. 7c. The moisture flux from the Arabian Sea that turns anticyclonically over the Arabian Peninsula and the westerly moisture flux coming from the Mediterranean Sea bring moisture to the western and southern part of Iran. Yuan et al. (2011) recently showed that the anticyclonic circulation is strengthened as a response to the diabatic heating above the Arabian Sea during the IOD.

Figure 7a shows the composite map for the moisture flux anomaly during the wet years. Here, wet (dry) years correspond to those years with the principal component of the first EOF mode for OND above 0.8 (below −0.8) standard deviation (see Table 4). The anomalous moisture flux anomaly from the Arabian Sea turning anticyclonically and that from the Red Sea converge and flow toward the southern part of Iran, causing more precipitation there. As shown in Fig. 8a, this is associated with a positive (negative) relative vorticity anomaly over both the eastern Mediterranean Sea and the north Red Sea (East Arabian Peninsula–Arabian Sea). These two systems help to transport more moisture to the southern part of Iran. Also, when the contribution from the anomalous advection of climatological moisture is compared with that from the climatological advection of anomalous moisture, it is found that the contribution from the former dominates (Fig. 10). On the other hand, the direction of moisture flux anomaly during dry years is almost opposite to that of wet years (Fig. 7a, b). This is associated with the northward shift of the Arabian anticyclone to the northern Red Sea (Fig. 8b). The SLP anomalies around the Bay of Bengal (northeast of Iran) are positive (negative) during wet years. The positive SLP anomaly shifts northward, whereas the negative anomaly is over the Mediterranean Sea for dry years (Fig. 9a, b).

Fig. 11 Composites of moisture flux anomaly in October–November of **a** positive and **b** negative IOD (Unit: kg m^{-1} s^{-1}, vectors are plotted only where they are significant at the 90 % confidence level) and moisture flux anomaly divergence (Unit: 10^{-4} kg m^{-2} s^{-1})

Since the DMI has a significant positive correlation with the first EOF mode during October and November, composites of moisture flux are constructed for positive and negative IOD events in October–November. Years in which the DMI is above (below) one standard deviation in October–November are selected to identify five positive (1977, 1982, 1994, 1997 and 2002) and three negative (1975, 1996 and 1998) IOD events. During the positive

IOD, the anomalous southeasterly moisture flux over the Arabian Sea turns anticyclonically and transport more moisture to the southern part of Iran from the Arabian Sea, the Red Sea, and the Persian Gulf (Fig. 11a). In contrast, the moisture flux has a small northerly anomaly over Iran during the negative IOD, which is indicative of reduced moisture supply from the south (Fig. 11b). The above moisture flux anomaly pattern for the positive (negative)
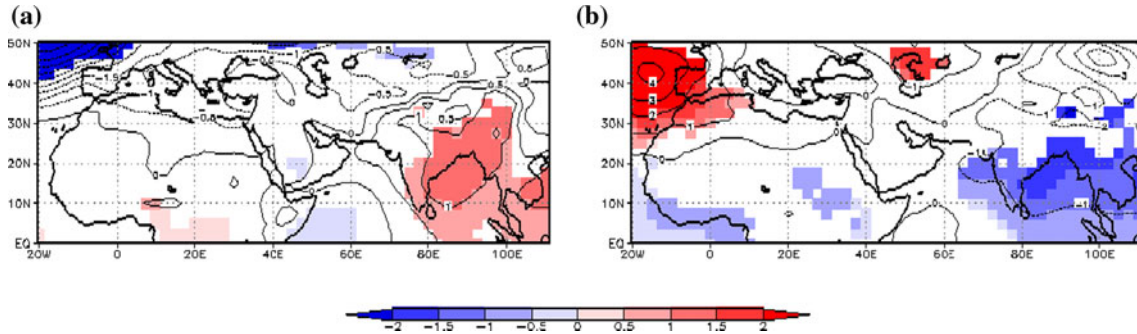

Fig. 12 Composites of SLP anomalies (in hPa) for **a** positive and **b** negative IOD. Anomalies exceeding 90 % confidence level are *shaded*

Fig. 13 Composites of moisture flux anomaly in JFMAM during **a** wet and **b** dry years (Unit: kg m^{-1} s^{-1}, vectors are plotted only where they are significant at the 90 % confidence level) and moisture flux anomaly divergence (Unit: 10^{-4} kg m^{-2} s^{-1}). **c** Climatology of moisture flux in JFMAM
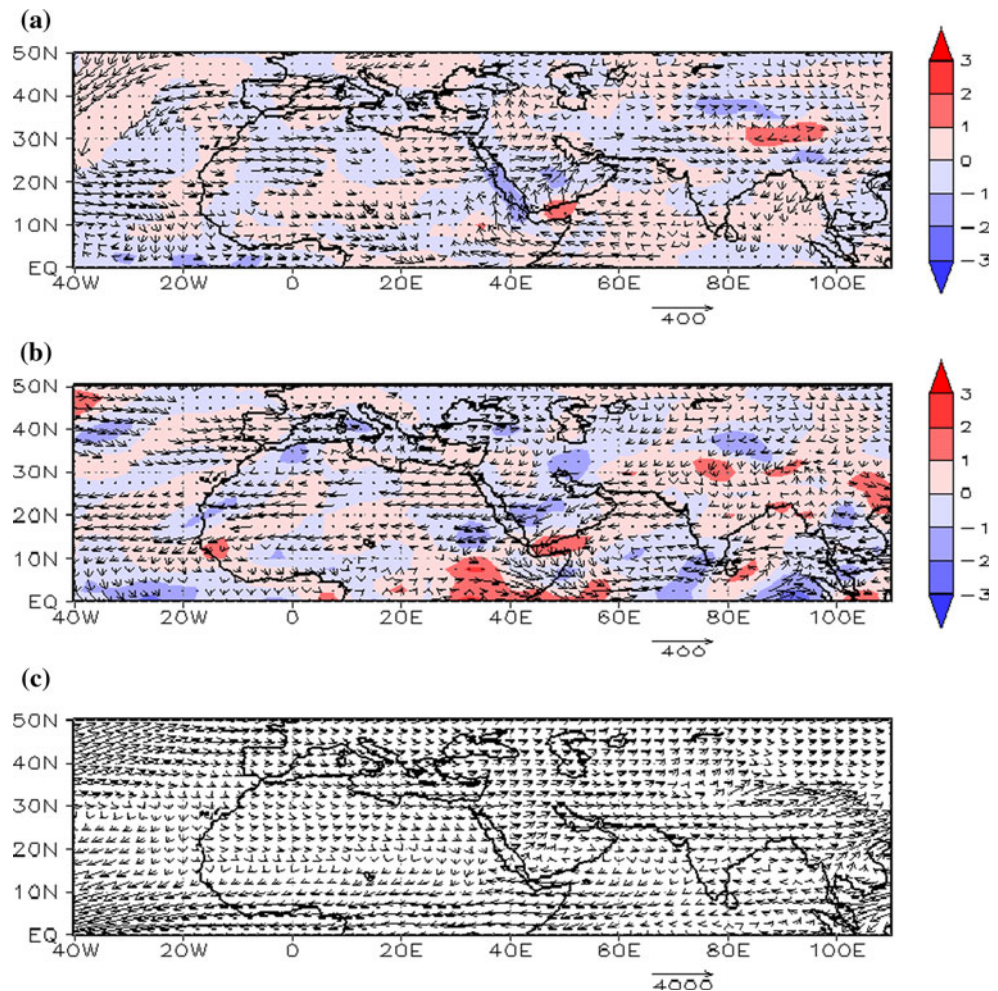
IOD resembles that of the wet (dry) years as expected. The SLP anomalies centered around the Bay of Bengal is positive (negative) during positive (negative) IOD events (Figs. 12a, b).

5.2 Second part of the rainy season (JFMAM)

In winter and spring, the Arabian anticyclone moves to the east and over the Arabian Sea (Raziei et al. 2011). Figure 13c shows the climatological moisture flux in JFMAM. The westerly moisture flux from the Mediterranean Sea and southwesterly moisture flux from the Red Sea and the Persian Gulf converge around the southern part of Iran.

In the composite of wet years (Fig. 13a), the westerly moisture flux anomaly from the Mediterranean Sea and the Red Sea and southwesterly moisture flux anomaly originating from the western tropical Indian Ocean are observed. These suggest that the moisture flux is enhanced as compared to the climatology such that the precipitation over the southern part of Iran increases. As shown in Fig. 10, the contribution from anomalous advection of climatological moisture is more dominant compared with that from the climatological advection of anomalous moisture. The positive (negative) relative vorticity anomaly over the western Mediterranean Sea (North Africa), as seen in Fig. 8c, suggests the possible role of the WeMO.

On the other hand, an easterly moisture flux anomaly is found over the southern part of Iran, and a northeasterly moisture flux anomaly is seen from the Persian Gulf to the Red Sea (Fig. 13b). These anomalies are opposite to the climatological flux, and are indicative of weakening in the climatological moisture transport during this season. The relative vorticity anomaly shown in Fig. 8d suggests that northward shift of the anticyclone over the Mediterranean Sea.

6 Conclusions

In this study, interannual variations of precipitation in the southern part of Iran are studied using reanalysis and rainfall station data from 1974 to 2005. Since the major part of precipitation in the southern part of Iran occurs during October to May, we have focused on these particular months. The first EOF explains more than 50 % of the total variance in precipitation anomaly from October to April and 38.8 % in May. The interannual variation of rainfall in October and November is more closely connected to IOD than ENSO. This is contrasted with the past studies suggesting that the interannual variation is caused by ENSO. This apparent discrepancy arises from the fact that some positive IOD and El Niño events co-occur. Since the IOD decays in boreal winter, this also explains why the

past studies found the correlation with ENSO only during boreal autumn even though canonical ENSO events peak in winter and stay even in spring. The moisture flux anomaly shows that the southeasterly anomaly over the Arabian Sea turns anti-cyclonically and transports more moisture to the southern part of Iran from the Arabian Sea, Red Sea, and Persian Gulf during the positive IOD. In contrast, the moisture flux has a northerly anomaly over Iran during the negative IOD, which signifies reduced moisture supply from the south. Therefore, it is important to pay more attention to the Indian Ocean when predicting the precipitation anomaly in the first part of the rainy season. On the other hand, the interannual variation of precipitation in the second part of the rainy season is more strongly influenced by a mode of variability in the Mediterranean Sea. The induced large-scale atmospheric circulation anomaly controls moisture supply from the Red Sea and the Persian Gulf.

The present research is based on analyses of the observational data using linear statistical methods. Further studies using GCM experiments are required to isolate influences of each of climate modes on the precipitation variation over Iran.

References

Ashok K, Guan Z, Yamagata T (2001) Impact of the Indian Ocean dipole on the relationship between the Indian Monsoon rainfall and ENSO. Geophys Res Lett 28:4499–4502

Ashok K, Guan Z, Yamagata T (2003) Influence of Indian Ocean Dipole on the Australian winter rainfall. Geophys Res Lett 30. doi:10.1029/2003GL0117926

Ashok K, Behera SK, Rao SA, Weng H, Yamagata T (2007) El Niño Modoki and its possible teleconnection. J Geophys Res 112. doi:10.1029/2006JC003798

Barnston AG, Livezey RE (1987) Classification, seasonality and persistence of low-frequency atmospheric circulation pattern. Mon Wea Rev 115:1083–1126

Chakraborty A, Behera SK, Mujumdar M, Ohba R, Yamagata T (2006) Diagnosis of tropospheric moisture over Saudi Arabia and influence of IOD and ENSO. Mon Wea Rev 134:598–617

Chiang JCH, Vimont DJ (2004) Analogous meridional modes of atmosphere-ocean variability in the tropical Pacific and tropical Atlantic. J Clim 17:4143–4158

Doi T, Tozuka T, Yamagata T (2010) The Atlantic meridional mode and its coupled variability with Guinea dome. J Clim 15:455–475

Domroes M, Kaviyani M, Schaefer D (1998) An analysis of regional and intra-annual precipitation variability over Iran using multivariate statistical methods. Theor Appl Climatol 61:151–159

England MH, Ummenhofer CC, Santoso A (2006) Interannual rainfall extremes over south west Western Australia linked to Indian Ocean climate variability. J Clim 19:1948–1969

Ghasemi AR (2003) Metrological drought in Iran and its association with El Niño-Southern Oscillation and Caspian Sea surface temperature. Dissertation, University of Shiraz

Ghasemi AR, Khalili D (2008) The association between regional and global atmospheric patterns and winter precipitation in Iran. Atmos Res 88:116–133

Kalnay E (1996) The NCEP/NCAR-40 year reanalysis project. Bull Am Meterol Soc 77:437–471

Martin-Vide J, Lopez-Bustins JA (2006) The western Mediterranean oscillation and rainfall in the Iberian Peninsula. Int J Climatol 26:1455–1475

Nazemosadat MJ (2001) Winter rainfall in Iran: ENSO and a loft wind interactions. Iran J Sci Technol 25:611–624

Nazemosadat MJ, Cordery I (2000) On the relationship between ENSO and autumn rainfall in Iran. Int J Climatol 20:47–61

Nazemosadat MJ, Ghasemi AR (2004) Quantifying the ENSO-related shifts in the intensity and arability of drought and wet periods in Iran. J Clim 17:4005–4018

Nazemosadat MJ, Samani N, Barry DA, Molaii Niko M (2006) ENSO forcing on climate changing in Iran: precipitation analysis. Iran J Sci Technol 30:555–565

Rayner NA et al. (2003) Global analyses of sea surface temperature, sea ice, and night marine air temperature since the late nineteenth century. J Geophys Res 108. doi:10.1029/2002JD002670

Raziei T, Mofidi A, Satos JA, Bordi I (2011) Spatial pattern and regimes of daily precipitation in Iran relation to large-scale atmospheric circulation. Int J Climatol. doi:10.1002/joc.2347

Saji NH, Yamagata T (2003) Possible impacts of Indian Ocean dipole mode events on global climate. Clim Res 25:151–169

Saji NH, Goswami BN, Vinayachandran PN, Yamagata T (1999) A dipole mode in the tropical Indian Ocean. Nature 401:360–363

Webster PJ, Moore AM, Loschnig JP, Leben RR (1999) Coupled ocean-atmosphere dynamics in the Indian Ocean during 1997–98. Nature 401:356–360

Weng H, Ashok K, Behera SK (2007) Impacts of recent El Niño Modoki on dry/wet conditions in the Pacific rim during boreal summer. Clim Dyn 29:113–129

Yamagata T, Behera SK, Luo JJ, Masson S, Jury MR, Rao SA (2004) Coupled ocean-atmosphere variability in the tropical Indian Ocean. In: Earth's climate: the ocean-atmosphere interaction. Geophys Monogr 147:189–211

Yang J, Liu Q, Xie SP, Liu Z, Wu L (2007) Impact of the Indian Ocean SST basin mode on the Asian summer monsoon. Geophys Res Lett 34. doi:10.1029/2006GL028571

Yuan C, Tozuka T, Miyasaka T, Yamagata T (2009) Respective influences of IOD and ENSO on the Tibetan snow cover in early winter. Clim Dyn 33:509–520. doi:10.1007/s00382-008-0495-2

Yuan C, Tozuka T, Yamagata T (2011) IOD influence on the early winter Tibetan Plateau snow cover: Diagnostic analyses and an AGCM simulation. Clim Dyn. doi:10.1007/s00382-011-1204-0

Zubair L, Andra S, Rao SA, Yamagata T (2003) Modulation of Sri Lanka Maha rainfall by Indian Ocean Dipole. Geophys Res Lett 30. doi:10.1029/2002GL05639